pubs.acs.org/Langmuir Article

In Situ Electrochemistry of Formate on Cu Thin Films Using ATR-FTIR Spectroscopy and X-ray Photoelectron Spectroscopy

Jason Hsu, Mohamed S. E. Houache, Yaser Abu-Lebdeh, Reagan A. Patton, Marcelo I. Guzman, and Hind A. Al-Abadleh*

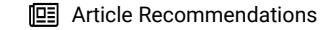


Cite This: Langmuir 2024, 40, 2377-2384

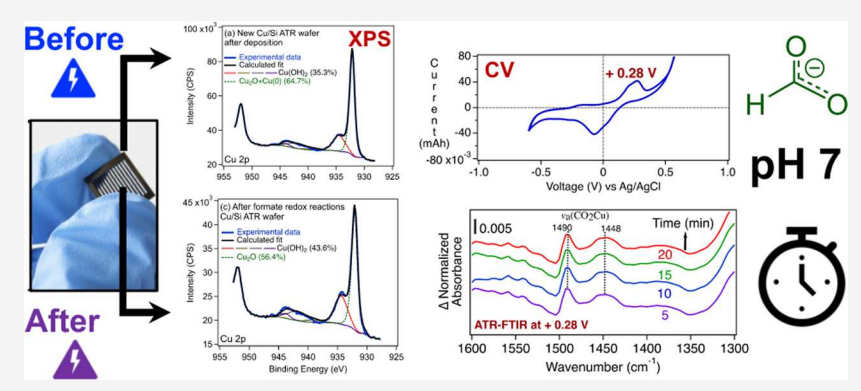


ACCESS

III Metrics & More



s Supporting Information



ABSTRACT: Formate (HCOO $^-$) is the most dominant intermediate identified during carbon dioxide electrochemical reduction (CO₂ER). While previous studies showed that copper (Cu)-based materials that include Cu(0), Cu₂O, and CuO are ideal catalysts for CO₂ER, challenges to scalability stem from low selectivity and undesirable products in the -1.0-1.0 V range. There are few studies on the binding mechanism of intermediates and products for these systems as well as on changes to surface sites upon applying potential. Here, we use an in situ approach to study the redox surface chemistry of formate on Cu thin films deposited on Si wafers using a VeeMAX III spectroelectrochemical (SEC) cell compatible with attenuated total reflectance Fourier transform infrared spectroscopy (ATR-FTIR). Spectra for surface species were collected in real time as a function of applied potential during cyclic voltammetry (CV) experiments. Results showed the reproducibility of CV curves on freshly prepared Cu/Si wafers with relatively high signal-to-noise ATR-FTIR absorbance features of surface species during these electrochemical experiments. The oxidation reaction of HCOO $^-$ to bicarbonate (HCO $_3$) was observed using ATR-FTIR at a voltage of 0.27 V. Samples were then subjected to reduction in the CV, and the aqueous phase products below the detection limit of the SEC-ATR-FTIR were identified using ion chromatography (IC). We report the formation of glycolate (H $_3$ C $_2$ O $_3$) and glyoxylate (HC $_2$ O $_3$) with trace amounts of oxalate (C $_2$ O $_4$ 2 $^-$), indicating that C $^-$ C coupling reactions proceed in these systems. Changes to the oxidation state of surface Cu were measured using X-ray photoelectron spectroscopy, which showed a reduction in Cu(0) and an increase in Cu(OH) $_2$, indicating surface oxidation.

INTRODUCTION

Past efforts to understand the mechanistic details of heterogeneous carbon dioxide (CO_2) electrochemical reduction (CO_2ER) on copper-based materials emphasized the role of reaction intermediates in forming the final products. ^{1–5} Among the most frequently observed intermediates in CO_2ER are bicarbonate (HCO_3^-)^{6,7} and formate ($HCOO^-$), which form directly from CO_2 in solution according to reactions $R1-R3^{4,7}$

$$CO_2(g) + H_2O(l) \rightleftharpoons H_2CO_3(aq) \rightleftharpoons HCO_3^-(aq) + H^+(aq),$$

 $Henry's Law constant, H_{CO_2(25^{\circ}C)} = 3.38 \times 10^{-2} \text{ mol L}^{-1} \text{ atm}^{-1}$
(R1)

$$CO_2(aq) + H^+(aq) + 2e^- \rightarrow HCOO^-(aq), \quad E_{red}^{\circ} = -0.63 \text{ V}$$
(R2)

$$\text{HCOO}^{-}(\text{aq}) + 3\text{OH}^{-}(\text{aq}) \rightleftharpoons \text{CO}_{3}^{2-}(\text{aq}) + 2\text{H}_{2}\text{O} + 2\text{e}^{-}$$

 $E_{\text{ox}}^{\circ} = 0.20 \text{ V}$ (R3)

Thin films and nanoparticles of copper (Cu)-based materials that include metallic Cu and oxidized copper, Cu₂O, and CuO demonstrated promising potential in forming useful products and fuels compared with precious metals such as platinum and

Received: November 27, 2023 Revised: January 2, 2024 Accepted: January 3, 2024 Published: January 17, 2024





palladium. $^{5,8-10}$ However, undesirable products form in the -1.0-1.0 V electrochemical potential range due to the low selectivity of these electrocatalysts. This issue with Cu-based materials poses the biggest challenge in CO_2ER for scalability to commercial scale. 1,5,11,12

The efficiency of the CO2ER depends on the surface properties of the Cu electrocatalysts such as site type, charge, and morphology. Molecules in the gas and liquid phases react with copper surface sites in the CO₂ER. These reactions change copper surface site speciation. For example, the dissociation of oxygen and water produces an oxide layer that terminates copper surfaces, as reported using ambient pressure X-ray absorption spectroscopy (XPS). 13,14 It is more challenging to characterize the surface of copper electrocatalysts under an applied potential in the presence of electrolytes. Electrochemical roughening of polycrystalline Cu electrodes, Cu(poly), was observed in acidic media and in the presence of chloride, which increased the <100> facets and defect sites at the expense of the <111> facets. Similar observations were reported upon potential cycling using copper and copper oxide electrode surfaces in neutral phosphate-buffered electrolyte solution from analyzing in situ surface X-ray diffraction. 16 The fact that the surfaces of copper electrodes used in CO₂ER are terminated with an oxide layer and increase in roughness with applied potential needs to be taken into account when investigating the mechanism of CO₂ER.⁵ In this context, published reports assume that CO₂ER intermediates interact directly with copper centers through forming metal-carbon and metal-oxygen bonds. 1,17,18 Recently, we showed using attenuated total internal reflection Fourier transform infrared spectroscopy (ATR-FTIR) that formate, bicarbonate, and acetate form mostly outer-sphere complexes mediated by hydrogen bonding with CuO nanoparticles. 19 Analysis of the desorption kinetics of the surface complexes of these molecules was reflective of the heterogeneity of sites that affect the strength of hydrogen bonding, highlighting its importance in the overall CO₂ER mechanism with oxidized Cu(II) materials.

The objective of our studies here is to explore the use of a commercial and surface-sensitive spectroelectrochemical cell (SEC-ATR-FTIR) to conduct systematic in situ experiments to identify surface complexes due to the redox chemistry of formate on Cu thin films. These experiments were coupled with XPS, scanning electron microscopy/energy-dispersive X-ray spectroscopy (SEM/EDX), and ion chromatography (IC) measurements to identify changes to the surface oxidation state of Cu, surface morphology, and aqueous phase composition, respectively. Coupling a spectroelectrochemical cell (SEC) to ATR-FTIR spectroscopy has been common for studying surface electrochemistry on metallic electrodes dating back to the nineties (see as examples -but not limited to- ref 20-22). Surface-enhanced infrared absorption has proven to be a powerful technique in identifying surface species on a number of metallic thin films. The Cu thin films used here were deposited on a Si wafer suitable for SEC-ATR-FTIR measurements and were characterized following deposition and after formate redox chemistry in solution using XPS and SEM/EDX. Water-soluble products were identified and quantified as well by IC with the alkanol quaternary ammonium column. Such a method is highly specific to separating monocarboxylic acids, dicarboxylic acids, and tricarboxylic acids, 23-29 resulting in an excellent approach to determine the soluble intermediates/ products from CO₂ reduction. Therefore, the results below provide not only method development for spectral collection of surface species using a commercial SEC-ATR-FTIR but also evidence for surface Cu oxidation, increased roughness, and C—C coupling reactions, producing C2—C4 products.

EXPERIMENTAL SECTION

Chemicals. Copper thin films (25 nm thickness) were deposited on Si wafers from copper nanoparticles (Kamis Inc. Cu 99.99%) with DC magnetron sputtering at the National Research Council (NRC) in Ottawa, Canada. The morphology and elemental composition of these thin films were characterized by using SEM/EDX. The Cu/Si wafers were chosen over Cu foil because the Si wafers were manufactured for the spectroelectrochemical studies using the commercial ATR-FTIR system utilized here. Aqueous phase solutions were freshly prepared using ultrapure water (18.2 M Ω cm) prior to the start of each experiment. Sodium formate (HCOONa, Sigma-Aldrich, MW 68.01 g mol⁻¹) solutions were prepared with no added electrolytes. Experiments designed for method development were conducted using the redox chemistry of 4-methoxypyridine (4MOP) on gold films on Si wafers (Au/Si) prepared at the University of Saskatchewan using indium tin oxides (Himet Materials, 90% In₂O₃, 10% SnO₂), KAuCl₄, and NaF (see the Supporting Information for additional details).³⁰ For IC experiments, standards included solutions of sodium formate (HCOONa, Acros Organics, 99%), sodium glyoxylate monohydrate (HC₂O₃Na·H₂O, Santa Cruz Biotechnology, 95%), sodium glycolate (H₃C₂O₃Na, Thermo Fisher Scientific, 98.6%), sodium oxalate (C2O4Na2, Alfa Aesar, 99.9%), and sodium bicarbonate (HCO3Na, Sigma-Aldrich, 100.0%). Additional details are provided in the Supporting Information.

SEC-ATR-FTIR Spectroscopy Experiments. Electrochemical and surface chemistry adsorption experiments were conducted using a Nicolet 8700 FTIR Spectrometer (Thermo Instruments) equipped with a mercury—cadmium—telluride (MCT-A) detector and an ATR VeeMAX III (Pike Technologies) accessory with a Jackfish spectroelectrochemical cell (Pike Technologies). A Squidstat potentiostat (Admiral Instruments) was used to control the applied voltages with an installed Squidstat program. N₂ gas was used as an inert purging gas to reduce dissolved oxygen in the electrolyte solutions. Additional details are provided in the Supporting Information.

XPS Measurements. For identifying the oxidation states of Cu, C, and O, XPS analyses of the as-deposited and reacted Cu/Si wafers were carried out with a Kratos AXIS Supra X-ray photoelectron spectrometer using a monochromatic Al K α source (15 mA, 15 kV) in the Surface Science Western Facility at Western University. Additional details are provided in the Supporting Information.

lon Chromatography (IC) Analysis. Five solution samples were shipped to the University of Kentucky for IC analysis labeled as follows: (A) water at pH 7, (B) 0.1 M formate at pH 7 (control before reaction), (C) reacted 0.1 M formate at pH 7 (with reaction products), (D) 50 ppb LiF, and (E) 50 ppb LiF with frozen HI. All five vials, labeled A through E, were analyzed by IC following a protocol previously established and highly selective for the identification of formate, ^{23,24} glycolate, ^{26,27} bicarbonate, ²⁸ and oxalate. ^{25–27} Additional details are provided in the Supporting Information.

RESULTS AND DISCUSSION

In this paper, results are presented in four main sections: method development using the redox chemistry of 4MOP on Au/Si ATR wafers; identification of surface species during spectroelectrochemical redox reactions of formate on Cu/Si thin films; characterization of Cu/Si thin films before and after spectroelectrochemical redox reactions of formate on Cu/Si thin films; and identification and quantification of aqueous phase products.

Method Development Using the Redox Chemistry of 4MOP on Au/Si ATR Wafers. The molecule 4MOP undergoes reversible potential-dependent adsorption on Au/Si wafer

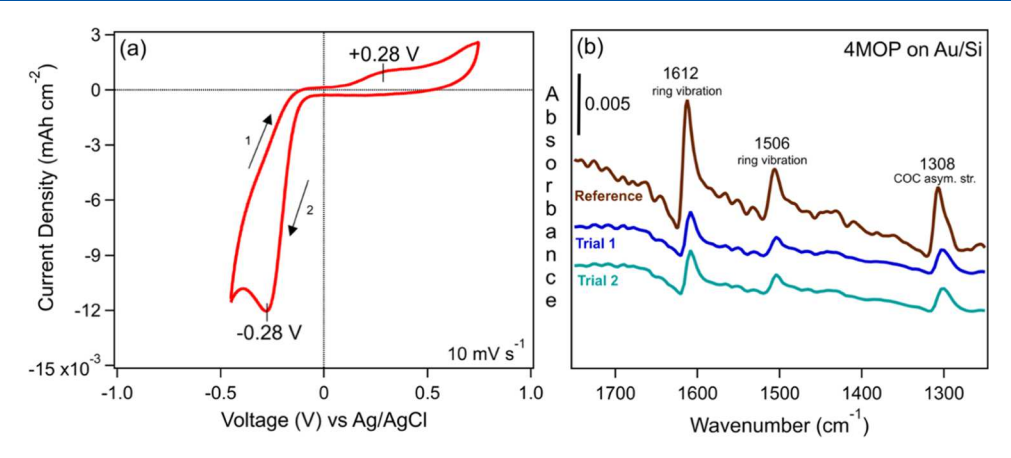


Figure 1. Electrochemical oxidation of 4MOP on Au/Si wafers using SEC-ATR-FTIR: (a) CV of 0.1 mM 4MOP adsorption in 0.1 M NaF on Au/Si ATR wafer at pH 7. (b) Comparison of SEC-ATR-FTIR spectra of 0.1 mM 4MOP adsorption in 0.1 M NaF on an Au/Si wafers at an electrical potential of +0.3 V (fully oxidized Au surface sites). These absorbance spectra were obtained by referencing the single beam spectra to the one collected at -0.9 V on an Au/Si ATR wafer (where Au surface sites exist as Au⁰). The "Reference" spectrum was obtained following Au deposition, courtesy of Ian Andvaag and Professor Ian Burgess of Jackfish SEC (University of Saskatchewan).

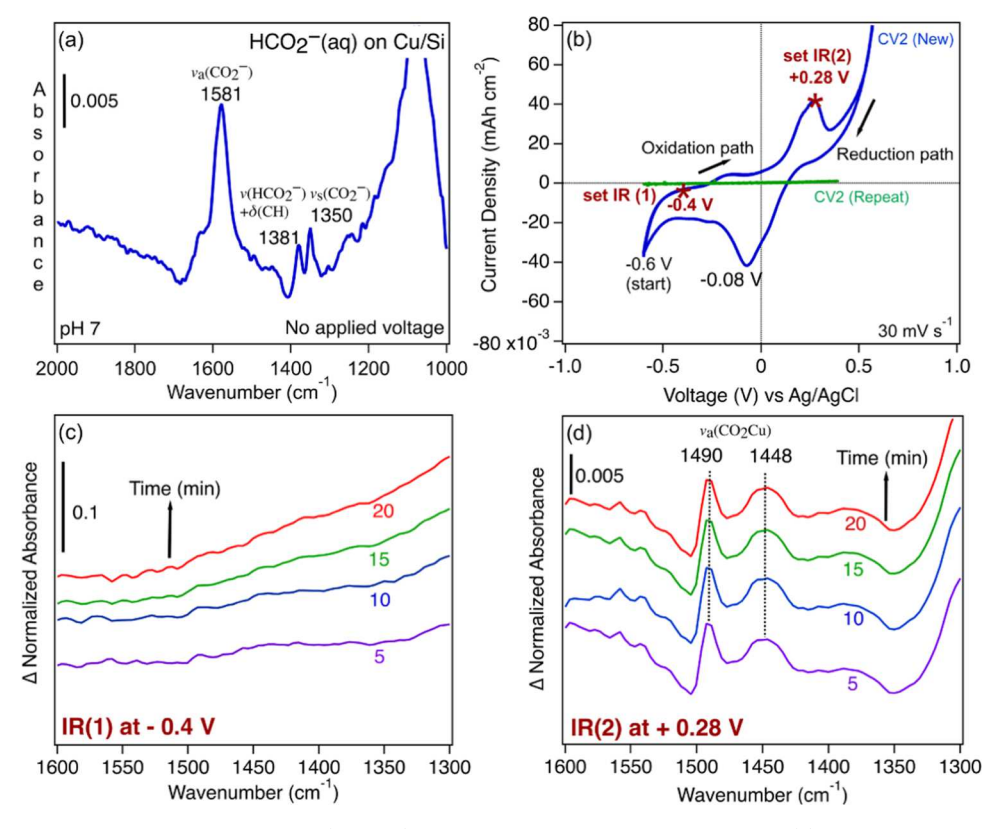


Figure 2. Electrochemical redox chemistry of formate (HCO_2^-) on Cu/Si wafers using SEC-ATR-FTIR: (a) representative absorbance spectrum of the starting solution, 0.1 M HCO_2^- , in the absence of applied potential. This spectrum was obtained by referencing the single beam spectrum to that recorded for background water at pH 7. (b) Representative CV curves for 0.1 M HCO_2^- at pH 7 on a wafer with a freshly deposited Cu thin film and a reacted Cu thin film following formate redox chemistry on the freshly deposited Cu thin film. Two sets of SEC-ATR-FTIR spectra were collected: set IR(1) at -0.4 V, where no redox chemistry was taking place and set IR(2) at +0.28 V, where oxidation was taking place at the anodic peak. (c) Representative set of IR(1) net normalized absorbance spectra collected at -0.4 V as a function of time obtained according to eq R4. (d) Representative set of IR(2) normalized absorbance spectra collected at +0.28 V as a function of time obtained according to eq R4. The assignment of spectral features in panel (a) and panel (d) is based on ATR-FTIR absorbance spectra recorded for formate and bicarbonate, respectively, in ref 19. The spectra in Figure 2c,d are offset from each other for clarity.

forming Au-(4MOP)₂ complexes according to reaction R4:^{31,32}

$$Au_{(s)}^{0} + 2(4MOP)_{(aq)} \rightleftharpoons Au - (4MOP)_{2(ads)}^{+} + e^{-}$$

$$E_{ox}^{\circ} = +0.12 \text{ V}$$
(R4)

The Au- $(4MOP)^+_{2(ads)}$ surface complexes have distinct IR spectral features, as reported from the SEIRAS spectra on gold film electrodes. Figure 1a shows the cyclic voltammogram (CV) for the adsorption of 4MOP (0.5 mM) in 0.1 M NaF on Au/Si ATR wafer at pH 7. The anodic peak is observed at +0.28,

indicating oxidation, whereas the cathodic peak around -0.28 V indicates reduction. The SEC-ATR-FTIR absorbance spectra collected at +0.3 V are shown in Figure 1b.

The spectra show the three most intense features attributed to Au-(4MOP)⁺_{2(ads)} surface complexes centered at 1612, 1506, and 1308 cm⁻¹. The first two spectral features were assigned to asymmetric and symmetric ring vibrations, respectively, and the latter one to the ester COC asymmetric stretch.³¹ These experiments were valuable in ensuring that the electrical connections within the SEC-ATR-FTIR accessory were intact and that it is a reliable tool for reproducing earlier published work prior to using it for new experiments with other chemicals and thin films, as described below, for formate on Cu/Si wafers.

Identification of Surface Species during Spectroelectrochemical Redox Reactions of Formate on Cu/Si Thin Films. The redox chemistry of formate per reaction R3 was monitored in situ and in real time using SEC-ATR-FTIR equipped with a freshly deposited Cu/Si ATR wafer. Figure 2a shows the starting absorbance spectrum of 0.1 M formate at pH 7 prior to applying potential. The relatively high formate concentration was used to generate detectable amounts of redox products in the online SEC-ATR-FTIR spectral recording and offline solution analysis of water-soluble products using IC. The observed spectral features at 1581, 1381, and 1350 cm⁻¹ are assigned to the vibrational modes of formate, the conjugated base of formic acid with p K_a 3.75.³³ We observed these spectral features on a ZnSe ATR internal reflection element in liquid H_2O at pH 7 at 1581, 1381, and 1350 cm⁻¹, and in liquid D_2O at pH 7 at 1589, 1385, and 1350 cm⁻¹. The same spectral features were observed for outer-sphere formate complexes on CuO nanoparticles at pH 7.19

Then, a potential was applied to the working electrode (Cu/Si wafer) starting at -0.6 V to collect the CV curve for formate. Figure 2b shows a representative CV curve for formate (0.1 M) at pH 7. The anodic peak for the oxidation of formate per reaction R3 was observed at +0.28 V, whereas the cathodic peak for formate reduction was observed at -0.08 V. Data reproducibility was studied on another freshly deposited Cu/ Si wafer by collecting additional CV curves, as shown in Figure S1. The first CV curve (CV2) showed the highest conductivity, followed by three CV curves (CV2-4) with progressively lower current. The fifth CV curve showed a -0.05 V shift in the anodic peak and a +0.25 V in the cathodic peak. Hence, it was inferred that the surface properties of the Cu/Si wafer were changing with consecutive CV cycles for formate redox chemistry. When comparing the CV curve in Figure 2b to CV2 in Figure S1, the data showed that the voltage of the anodic peak at +0.28 V shifted by 0.1 to +0.38 V and that the cathodic peaks appeared at a lower voltage, -0.08 V, similar to the one observed for CV3-5. The variability in the shape of the CV curves and magnitude of the current indicated nonuniformity in the deposition of the Cu thin films on the Si wafer, even though the procedure of the thinfilm deposition was automated. These studies clearly suggest that for IR spectra to be collected at a given voltage that corresponds to either oxidation or reduction on the Cu thin film, the Cu/Si wafer should not be subjected to more than three cycles of CV curve collections.

Once the locations of the anodic and cathodic peaks were identified from the CV curve shown in Figure 2b, two sets of SEC-ATR-FTIR spectra were collected as a function of time at two voltage values: set IR(1) at -0.4 V, where no redox chemistry is expected, and set IR(2) at +0.28 V. Figure S2 shows the absorbance spectra of each set of IR spectra as a function of

time from the start of applying potential. These spectra were obtained by referencing the single beam spectra to the one recorded for 0.1 M formate at 0 V. This method of referencing would cancel out the features assigned to formate shown in Figure 1a. The 2000-1300 cm⁻¹ spectral range contains fundamental vibrational modes for most organic functional groups and the bending mode of water, $\delta(H_2O)$. The absorbance spectra in Figure S2a showed no detectable new peaks attributed to organic species, which is expected at -0.4 V. However, there was a net positive absorbance at 1630 cm⁻¹ for $\delta(H_2O)$, suggesting an increase in the surface water concentration. For comparison, the absorbance spectra in Figure S2b showed new peaks at 1490 and 1448 cm⁻¹ assigned to $v(CO_2Cu)$. These features were observed before for the solution containing 1:1 $Cu(II) + [HCO_3^-](aq)$ at pH 4.8. ¹⁹ Also, we reported that inner-sphere monodentate carbonate complexes on CuO nanoparticles were characterized by spectral features at 1489 and 1362 cm⁻¹, whereas physisorbed bicarbonate species were characterized by the 1612 and 1412 cm⁻¹ peaks. ¹⁹ The latter had a net positive absorbance at 1635 cm⁻¹ for $\delta(H_2O)$, suggesting an increase in the surface water concentration.

In order to amplify the spectral features assigned to $\nu(\text{CO}_2\text{Cu})$ from the oxidation products of formate at +0.28 V, each absorbance spectrum in Figure S2a,b was normalized to the absorbance at $\delta(\text{H}_2\text{O})$ in the same spectrum. Then, the normalized absorbance spectrum of the background liquid water collected at the beginning of the experiments was subtracted out to remove the $\delta(\text{H}_2\text{O})$, according to eqs 1 and 2

$$A_{\text{norm},-0.4V} = \frac{A_{-0.4V}(\nu, t)}{A_{-0.4V}(1630, t)} - \frac{A_{0V,H_2O}(\nu)}{A_{0V,H_2O}(1630)}$$
(1)

$$A_{\text{norm,0.28V}} = \frac{A_{0.28V}(\nu, t)}{A_{0.28V}(1635, t)} - \frac{A_{0V,H_2O}(\nu)}{A_{0V,H_2O}(1635)}$$
(2)

The resulting net normalized absorbance spectra are shown in Figure 2c,d. Similar to the observations made in Figure S2a,b, the spectra in Figure 2c,d showed neither features attributed to organic products at -0.4 V nor amplified new peaks at 1490 and 1448 cm⁻¹ assigned to $\nu(\text{CO}_2\text{Cu})$. The 1362 cm⁻¹ feature observed in the case of bicarbonate adsorption on CuO nanoparticles was not clear in the spectra in Figures 2d and S2b, and the 1612 cm⁻¹ peak was not isolated after subtracting the broad and intense $\delta(H_2O)$ peak. These differences in the observed spectral features of bicarbonate surface complexes on the Cu/Si thin film and CuO nanoparticles reflected the differences in surface sites and oxidation states of Cu in both materials. Also, there was an apparent lack of time dependence of the spectra in Figure 2d, suggesting that the formation of the adducts detected in the aqueous phase using IC happened very quickly (see below). The following section describes the characterization of Cu/Si thin films, freshly deposited and following redox chemistry with formate, for comparison with the surface characterization of CuO nanoparticles reported earlier. 19

Morphology and XPS Characterization of Cu/Si ATR Wafers before and after Spectroelectrochemical Redox Reactions of Formate. Figure S3a,b shows SEM/EDX images and spectra with % weight of elements in different areas across the Cu/Si wafers after deposition and following redox chemistry with formate, respectively. There is a clear morphological change due to surface electrochemistry accompanied by a nonuniform decay in the % weight of Cu and an increase in the % weight of C in some areas. This analysis explained the gradual

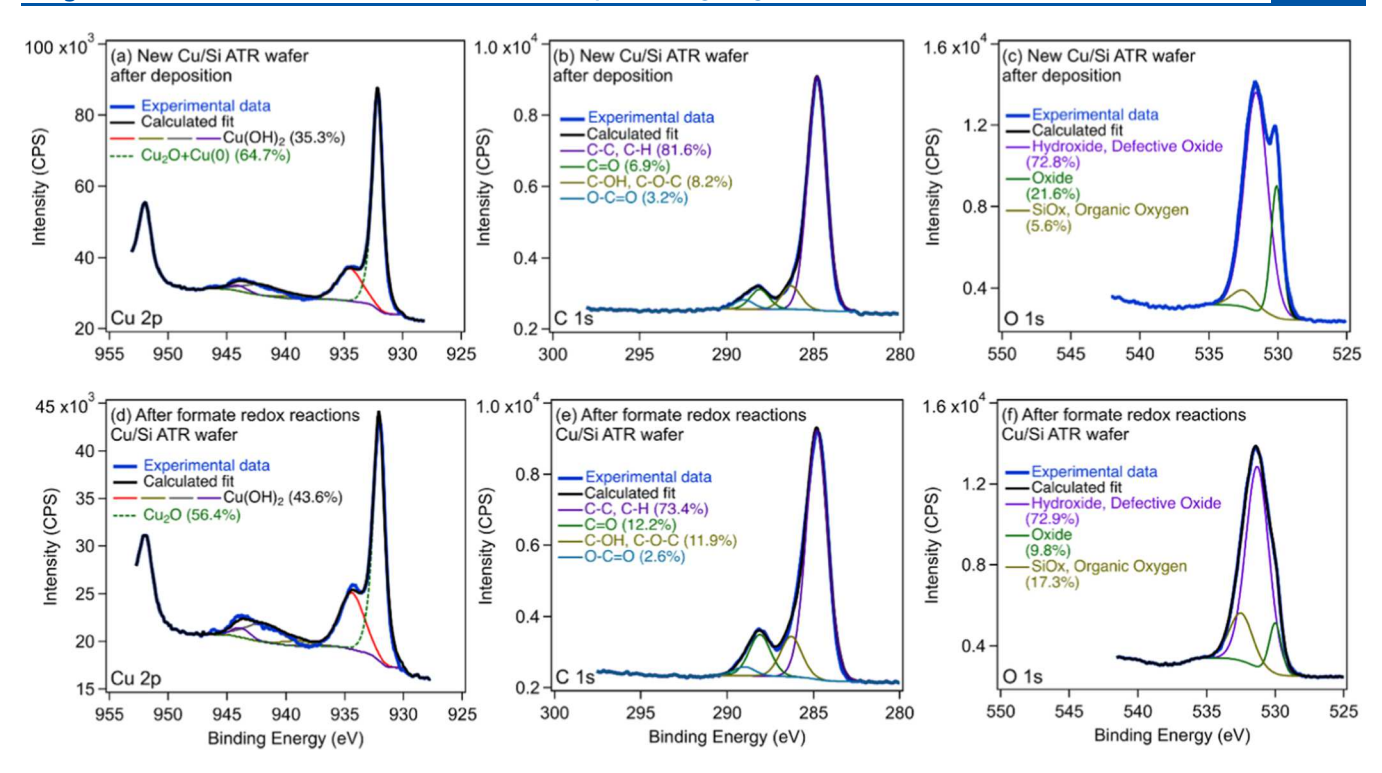


Figure 3. XPS spectra of Cu/Si wafers used in our studies, with peak fittings assigned to functional groups. Results of the peak fittings are listed in the legend as % area.

reduction in the conductivity of the Cu thin films observed with multiple CV cycles, as shown in Figure S1.

Figure 3 shows the XPS spectra and results of peak fittings aimed at identifying the oxidation state and speciation of the Cu, C, and O elements at the surfaces of these Cu/Si ATR wafers. Figure 3a-c shows the XPS Cu 2p, C 1s, and O 1s spectra, respectively, for a new wafer after deposition of the Cu thin film. The peak fittings indicated the presence of 64.7% Cu(0) + Cu(I) and 35.3% Cu(II) in the form of Cu(OH)₂. The majority, 81.6%, of the C speciation is in the form of C-C and C-H with some oxidized functional groups. These species were likely from adventitious carbon from handling the wafers and exposure to ambient conditions. As stated in the Supporting Information, the freshly deposited thin films did not undergo cleaning to remove excess carbon because our goal was to conduct experiments under realistic conditions that potentially mimic larger-scale systems for industrial applications. The peak fittings in the O 1s spectra showed that only 5.6% was due to either the underlying substrate (SiOx) or organic oxygen. The majority of the XPS signal of the o 1s was due to the presence of O in hydroxide or defective oxide (72.8%) and oxide (21.6%) of (most likely) the Cu film.

Figure 3d,e shows XPS spectra of reacted Cu/Si ATR wafers, highlighting the absence of Cu(0), a decrease in the relative amount of Cu(I), and an increase in the relative amount of Cu(II) to 43.6%. The direct evidence of the oxidation of Cu(0) is shown in Figure S4 for the Cu Auger peaks (Cu LMM) in the XPS spectra before and after the redox reaction of formate on the Cu/Si ATR wafer. Figure S4a shows that the new Cu/Si ATR wafer contained 10% of the Cu(0) along with 61% Cu(I) and 29% Cu(II), whereas after formate redox reactions, the Cu(0) peaks in Figure S4b disappeared, Cu(I) decreased to 49%, and Cu(II) increased to 51%.

Similarly, the C 1s spectra showed a near doubling in the C= O species to 12% and an increase in C-OH and C-O-C to

8.2%. Figure 3f shows a reduction in the % peak area of "oxide" to 9.8% and an increase in the % peak area of "SiOx, organic oxygen" to 17.3%. These results suggested irreversible changes to the surface structure of Cu thin films that affected the conductivity of the Cu/Si ATR wafers as working electrodes. The evidence for the loss of conductivity is shown in the green trace in Figure 2b labeled "CV2 (repeat)" with no current. Progressive reduction in the recorded current is also shown in Figure S1, indicating irreversibility of the redox chemistry. The interpretation of the XPS results could explain how the change from Cu(0) to Cu(II) during the reduction step in Figure 2b produced not only formate per reaction R3 (see the Introduction section) but also other C2 aqueous phase products, indicating C-C coupling reactions (see below). The implications of these findings are detailed below in the Conclusions and Significance section. Although Cu-oxides are converted to metallic Cu during CO2ER, these changes are not reversible due to chemical and structural changes of the interface, with impacts on efficiency and product selectivity.

Identification and Quantification of Aqueous Phase Products. Seven anions were detected after the electrochemical treatment in the aqueous sample C by ion chromatography: (1) formate, (2) fluoride, (3) glycolate, (4) chloride, (5) glyoxylate, (6) bicarbonate, and (7) oxalate. The retention time for each species under present chromatographic conditions is provided in Table 1.

Quantifications were possible with calibration curves based on the analysis of three replicates. The amount of formate remaining in sample C relative to its original concentration in sample A totaled 54%, meaning that 46.0 (± 2.1) mM formate was lost during the electrochemical reaction (conversion of aqueous sample B to C). The growth of bicarbonate in sample C represented 0.86 (± 0.03) mM. The concentrations of produced glycolate and glyoxylate were 640 (± 20) and 95 (± 5) μ M,

Table 1. Chromatographic Peak Number, Retention Time (R.T.), and Name of Species in the Aqueous Sample C

peak #	R.T. (min)	compound
1	2.22	formate
2	3.10	fluoride
3	6.83	glycolate
4	10.43	chloride
5	14.22	glyoxylate
6	14.85	bicarbonate
7	15.27	oxalate

respectively. The trace of oxalate formed in sample (C) was 1.3 $(\pm 0.2)~\mu M$.

Scheme 1 displays the proposed electrochemical reactions observed when a potential was applied to the formate solution.

Scheme 1. Proposed Electrochemical Reactions Starting from Formate Intermediate

Formate

$$CO_2 + 2e^- + H^+$$
 $CO_2 + 2e^- + 2H^+$
 $R6 - HCO_3^- + H^+$
 $CO_2 + 2e^- + 2H^+$
 $R7 - CO + H_2O$
 $2e^- + 2H^+$
 $R8 - H_2$
 $2CO_2 + 2e^ CO_2 + 2e^-$

During oxidation, formate is converted quickly to CO₂, which creates the bicarbonate surface complexes detected in our work by consecutive reactions R5 and R6 in Scheme 1, respectively. Although not observed here, Scheme 1 includes reactions for the reduction of CO₂ to carbon monoxide (R7) and hydrogen evolution by R8.

The recombination of two reduced CO_2 species creates oxalic acid by half-reaction R9, which acts as the precursor for the reductive generation of glyoxylate and glycolate in R10 and R11, respectively. It must be noted that the production of oxalate may involve different steps, including an initial one-electron transfer to CO_2 and radical—radical dimerization of $\mathrm{CO}_2^{-\bullet}$. The products of reactions R9, R10, and R11 demonstrate that C—C coupling reactions were accomplished.

CONCLUSIONS AND SIGNIFICANCE

Mechanistic details of the surface chemistry of Cu-based materials as the most versatile electrocatalysts in the $\rm CO_2ER$ are lacking, which makes it challenging to optimize conditions for scalability. Here, we reported spectroelectrochemical data on the redox chemistry of formate as the most commonly detected intermediate on Cu thin films using a commercially available

SEC-ATR-FTIR designed for studying electrochemical processes in solution. These measurements were coupled with surface characterization of Cu thin films before and after the redox chemistry with formate using SEM/EDX and XPS, followed by water-soluble product identification using IC. The results indicated that while formate formed outer-sphere complexes with surface sites on the Cu thin films, it got oxidized to form inner-sphere bicarbonate. The reduction step resulted in forming several low-molecular-weight organic compounds with C–C bonds. The oxidation—reduction cycles of formate resulted in morphological changes to the deposited Cu thin films and an irreversible increase in Cu(I) and Cu(II) surface sites at the expense of Cu(0), which reduced the conductivity of the Cu thin films and rendered the Cu/Si ATR wafers nonreusable for repeat experiments.

The results of this study are significant, as they are the first systematic set of experiments conducted in situ and in real time with a single intermediate, formate, as the major CO2ER intermediate on Cu thin films using SEC-ATR-FTIR. Coupling ATR-FTIR spectroscopy with electrochemistry and surface site characterization before and after proved powerful in obtaining mechanistic insights into this process. The chemical implications of these results highlighted that a single intermediate can produce several reduction products with irreversible changes to morphology and surface speciation that reduce conductivity. These findings originate from the fact that outer-sphere surface complexes of formate are dominant on copper surfaces containing mostly oxidized Cu(I) and Cu(II) sites. Hence, hydrogen bonding plays a major role in driving unselective product formation. Future surface-sensitive and theoretical studies are needed to explore the optimum time and cost associated with preparing metallic thin films on Si wafers, investigate the spectroelectrochemical processes of the other major intermediates bicarbonate and acetate, and unravel how charge screening/reversal from added electrolytes would influence the binding affinities of these intermediates and distribution of reduction products. Future experimental and computational methodologies need to simulate the liquid/solid interface and terminations of surface sites under realistic CO₂ER reaction conditions.

ASSOCIATED CONTENT

Supporting Information

This material is available free of charge via the Internet. The Supporting Information is available free of charge at https://pubs.acs.org/doi/10.1021/acs.langmuir.3c03660.

Figures and tables showing details on the experimental methods; preparation; and characterization of the Cu/Si wafers; consecutive CV cycles for 0.1 M formate at pH 7 on freshly deposited Cu/Si wafer; additional SEC-ATR-FTIR spectra for the redox chemistry of 0.1 M formate; SEM/EDX images and spectra of the Cu/Si wafers; and XPS spectra of Cu/Si wafers (PDF)

AUTHOR INFORMATION

Corresponding Authors

Marcelo I. Guzman – Department of Chemistry, University of Kentucky, Lexington, Kentucky 40506, United States;

orcid.org/0000-0002-6730-7766; Email: marcelo.guzman@uky.edu

Hind A. Al-Abadleh – Department of Chemistry and Biochemistry, Wilfrid Laurier University, Waterloo, Ontario,

Canada K1A 0R6; orcid.org/0000-0002-9425-0646; Email: halabadleh@wlu.ca

Authors

Jason Hsu – Department of Chemistry and Biochemistry, Wilfrid Laurier University, Waterloo, Ontario, Canada K1A 0R6

Mohamed S. E. Houache – National Research Council of Canada, Energy, Mining and Environment, Ottawa, Ontario, Canada K1A 0R6

Yaser Abu-Lebdeh — National Research Council of Canada, Energy, Mining and Environment, Ottawa, Ontario, Canada K1A 0R6; ⊙ orcid.org/0000-0001-8936-4238

Reagan A. Patton — Department of Chemistry, University of Kentucky, Lexington, Kentucky 40506, United States;
orcid.org/0009-0006-8775-3364

Complete contact information is available at: https://pubs.acs.org/10.1021/acs.langmuir.3c03660

Author Contributions

^{II}J.H. and R.A.P. contributed equally to the experimental work. **Notes**

The authors declare no competing financial interest.

ACKNOWLEDGMENTS

H.A.A. acknowledges partial funding from the NRC, NSERC, and Laurier's graduate scholarships to J.H. The authors are grateful to Ian Burgess and Ian Andvaag at the University of Saskatchewan and Jackfish SEC Manufacturing for gold thinfilm deposition and fruitful discussions on the setup and troubleshooting. The authors also thank Dr. Mark Biesinger at Surface Science Western at Western University for help in collecting the XPS data described in this paper. Funding from the U.S.A. National Science Foundation (NSF) under award 1903744 to M.I.G is greatly acknowledged. Support from a University of Kentucky NSF Research Traineeship Fellowship to R.A.P. under NSF award 1922694 is acknowledged.

REFERENCES

- (1) Zhu, S.; Li, T.; Cai, W. B.; Shao, M. CO2 Electrochemical Reduction As Probed through Infrared Spectroscopy. *ACS Energy Lett.* **2019**, *4* (3), 682–689, DOI: 10.1021/acsenergylett.8b02525.
- (2) Katayama, Y.; Nattino, F.; Giordano, L.; Hwang, J.; Rao, R. R.; Andreussi, O.; Marzari, N.; Shao-Horn, Y. An In Situ Surface-Enhanced Infrared Absorption Spectroscopy Study of Electrochemical CO2 Reduction: Selectivity Dependence on Surface C-Bound and O-Bound Reaction Intermediates. *J. Phys. Chem. C* 2019, 123 (10), 5951–5963, DOI: 10.1021/acs.jpcc.8b09598.
- (3) Moradzaman, M.; Mul, G. Infrared Analysis of Interfacial Phenomena during Electrochemical Reduction of CO2 over Polycrystalline Copper Electrodes. *ACS Catal.* **2020**, *10* (15), 8049–8057, DOI: 10.1021/acscatal.0c02130.
- (4) Chernyshova, I. V.; Somasundaran, P.; Ponnurangam, S. On the origin of the elusive first intermediate of CO2 electroreduction. *Proc. Natl. Acad. Sci. U.S.A.* **2018**, *115* (40), E9261–E9270, DOI: 10.1073/pnas.1802256115.
- (5) Wang, S.; Kou, T.; Baker, S. E.; Duoss, E. B.; Li, Y. Recent progress in electrochemical reduction of CO2 by oxide-derived copper catalysts. *Mater. Today Nano* **2020**, *12*, No. 100096.
- (6) Welch, A. J.; Dunn, E.; DuChene, J. S.; Atwater, H. A. Bicarbonate or Carbonate Processes for Coupling Carbon Dioxide Capture and Electrochemical Conversion. *ACS Energy Lett.* **2020**, *5* (3), 940–945, DOI: 10.1021/acsenergylett.0c00234.

- (7) Reddy, S. K.; Balasubramanian, S. Carbonic acid: molecule, crystal and aqueous solution. *Chem. Commun.* **2014**, *50* (5), 503–514, DOI: 10.1039/C3CC45174G.
- (8) Raciti, D.; Wang, C. Recent Advances in CO2 Reduction Electrocatalysis on Copper. ACS Energy Lett. 2018, 3 (7), 1545–1556.
- (9) Nitopi, S.; Bertheussen, E.; Scott, S. B.; Liu, X.; Engstfeld, A. K.; Horch, S.; Seger, B.; Stephens, I. E. L.; Chan, K.; Hahn, C.; et al. Progress and Perspectives of Electrochemical CO2 Reduction on Copper in Aqueous Electrolyte. *Chem. Rev.* **2019**, *119* (12), 7610–7672, DOI: 10.1021/acs.chemrev.8b00705.
- (10) Perry, S. C. Electrochemical Carbon Dioxide Reduction; de Gruyter, Berlin/Boston, 2021.
- (11) Papasizza, M.; Cuesta, A. In Situ Monitoring Using ATR-SEIRAS of the Electrocatalytic Reduction of CO2 on Au in an Ionic Liquid/Water Mixture. ACS Catal. 2018, 8 (7), 6345–6352.
- (12) Wu, J.; Huang, Y.; Ye, W.; Li, Y. CO2 Reduction: From the Electrochemical to Photochemical Approach. *Adv. Sci.* **2017**, *4* (11), No. 1700194.
- (13) Liu, B. H.; Huber, M.; van Spronsen, M. A.; Salmeron, M.; Bluhm, H. Ambient pressure X-ray photoelectron spectroscopy study of room-temperature oxygen adsorption on Cu(100) and Cu(111). *Appl. Surf. Sci.* **2022**, 583, No. 152438.
- (14) Trotochaud, L.; Head, A. R.; Pletincx, S.; Karslioğlu, O.; Karslioğlu, O.; Yu, Y.; Waldner, A.; Kyhl, L.; Hauffman, T.; Terryn, H.; Eichhorn, B. Water Adsorption and Dissociation on Polycrystalline Copper Oxides: Effects of Environmental Contamination and Experimental Protocol. J. Phys. Chem. B 2018, 122 (2), 1000–1008.
- (15) Sebastián-Pascual, P.; Escudero-Escribano, M. Surface characterization of copper electrocatalysts by lead underpotential deposition. *J. Electroanal. Chem.* **2021**, 896, No. 115446.
- (16) Grunder, Y.; Beane, J.; Kolodziej, A.; Lucas, C. A.; Rodriguez, P. Potential Dependent Structure and Stability of Cu(111) in Neutral Phosphate Electrolyte. *Surfaces* **2019**, 2 (1), 145–158.
- (17) Katayama, Y.; Nattino, F.; Giordano, L.; Hwang, J.; Rao, R. R.; Andreussi, O.; Marzari, N.; Shao-Horn, Y. An in Situ Surface-Enhanced Infrared Absorption Spectroscopy Study of Electrochemical CO2 Reduction: Selectivity Dependence on Surface C-Bound and O-Bound Reaction Intermediates. J. Phys. Chem. C 2018, 123 (10), 5951–5963.
- (18) Choi, C.; Kwon, S.; Cheng, T.; Xu, M.; Tieu, P.; Lee, C.; Cai, J.; Lee, H. M.; Pan, X.; Duan, X.; et al. Highly active and stable stepped Cu surface for enhanced electrochemical CO2 reduction to C2H4. *Nat. Catal.* **2020**, 3 (10), 804–812, DOI: 10.1038/s41929-020-00504-x.
- (19) Hsu, J.; Eid, A. M.; Randall, C.; Houache, M.; Abu-Lebdeh, Y.; Al-Abadleh, H. A. Mechanistic In-Situ ATR-FTIR Studies on the Adsorption and Desorption of Major Intermediates in CO2 Electrochemical Reduction on CuO Nanoparticles. *Langmuir* **2022**, 38 (48), 14789–14798.
- (20) Osawa, M. Dynamic Processes in Electrochemical Reactions Studied by Surface-Enhanced Infrared Absorption Spectroscopy (SEIRAS). *Bull. Chem. Soc. Jpn.* **1997**, 70 (12), 2861–2880.
- (21) Bae, I. T.; Barbour, R. L.; Scherson, D. A. In Situ Fourier Transform Infrared SpectroscopicStudies of Nitrite Reduction on PlatinumElectrodes in Perchloric Acid. *Anal. Chem.* **1997**, *69* (2), 249–252, DOI: 10.1021/ac960769n.
- (22) Climent, V.; Rodes, A.; Orts, J. M.; Feliu, J. M.; Perez, J. M.; Aldaz, A. On the Electrochemical and in-Situ Fourier Transform Infrared Spectroscopy Characterization of Urea Adlayers at Pt(100) Electrodes. *Langmuir* 1997, 13 (8), 2380–2389.
- (23) Zhou, R.; Guzman, M. I. Co2 reduction under periodic illumination of zns. J. Phys. Chem. C 2014, 118 (22), 11649–11656.
- (24) Rana, M. S.; Guzman, M. I. Surface Oxidation of Phenolic Aldehydes: Fragmentation, Functionalization, and Coupling Reactions. *J. Phys. Chem. A* **2022**, *126* (37), 6502–6516.
- (25) Zhou, R.; Guzman, M. I. Photocatalytic reduction of fumarate to succinate on ZnS mineral surfaces. *J. Phys. Chem. C* **2016**, *120* (13), 7349–7357.
- (26) Xia, S. S.; Eugene, A. J.; Guzman, M. I. Cross Photoreaction of Glyoxylic and Pyruvic Acids in Model Aqueous Aerosol. *J. Phys. Chem.* A **2018**, *122* (31), 6457–6466.

- (27) Eugene, A. J.; Xia, S. S.; Guzman, M. I. Aqueous Photochemistry of Glyoxylic Acid. *J. Phys. Chem. A* **2016**, 120 (21), 3817–3826.
- (28) Eugene, A. J.; Guzman, M. I. Reply to "Comment on 'Reactivity of Ketyl and Acetyl Radicals from Direct Solar Actinic Photolysis of Aqueous Pyruvic Acid". J. Phys. Chem. A 2017, 121 (15), 2924–2935.
- (29) Pillar-Little, E. A.; Zhou, R.; Guzman, M. I. Heterogeneous Oxidation of Catechol. *J. Phys. Chem. A* **2015**, *119* (41), 10349–10359.
- (30) Sigrist, J. A.; Lins, E. S.; Morhart, T. A.; Briggs, J. L.; Burgess, I. J. Optimization of a commercial variable angle accessory of entry level users of electrochemical attenuated total reflectaion surface-enhanced infrared absorption spectrscopy (ATR-SEIRAS). *Appl. Spectrosc.* **2019**, 73 (12), 1394–1402.
- (31) Quirk, A.; Unni, B.; Burgess, I. J. Surface Enhanced Infrared Studies of 4-Methoxypyridine Adsorption on Gold Film Electrodes. *Langmuir* **2016**, 32 (9), 2184–2191, DOI: 10.1021/acs.langmuir.5b04178.
- (32) Andvaag, I. R.; Morhart, T. A.; Clarke, O. J. R.; Burgess, I. J. Hybrid Gold—Conductive Metal Oxide Films for Attenuated Total Reflectance Surface Enhanced Infrared Absorption Spectroscopy. *ACS Appl. Nano Mater.* **2019**, 2 (3), 1274–1284.
- (33) Lide, D. R. CRC Handbook of Chemistry and Physics, 85th ed.; Taylor & Francis, 2004; Vol. 85.